THE JOURNAL OF BIOLOGICAL CHEMISTRY VOL. 284, NO. 20, pp. 13823–13831, May 15, 2009
© 2009 by The American Society for Biochemistry and Molecular Biology, Inc. Printed in the U.S.A.

Life and Death of Sensory Hair Cells Expressing Constitutively Active TRPML3*[S]

Received for publication, December 1, 2008, and in revised form, March 17, 2009 Published, JBC Papers in Press, March 19, 2009, DOI 10.1074/jbc.M809045200

Christian Grimm[1], **Simone Jörs**[1], **and Stefan Heller**[2]

From the Departments of Otolaryngology-Head and Neck Surgery and Molecular and Cellular Physiology, Stanford University School of Medicine, Stanford, California 94305-5739

The varitint-waddler mutation A419P renders TRPML3 constitutively active, resulting in cationic overload, particularly in sustained influx of Ca^{2+}. TRPML3 is expressed by inner ear sensory hair cells, and we were intrigued by the fact that hair cells are able to cope with expressing the TRPML3(A419P) isoform for weeks before they ultimately die. We hypothesized that the survival of varitint-waddler hair cells is linked to their ability to deal with Ca^{2+} loads due to the abundance of plasma membrane calcium ATPases (PMCAs). Here, we show that PMCA2 significantly reduced $[Ca^{2+}]_i$ increase and apoptosis in HEK293 cells expressing TRPML3(A419P). The deaf-waddler isoform of PMCA2, operating at 30% efficacy, showed a significantly decreased ability to rescue the Ca^{2+} loading of cells expressing TRPML3(A419P). When we combined mice heterozygous for the varitint-waddler mutant allele with mice heterozygous for the deaf-waddler mutant allele, we found severe hair bundle defects as well as increased hair cell loss compared with mice heterozygous for each mutant allele alone. Furthermore, 3-week-old double mutant mice lacked auditory brainstem responses, which were present in their respective littermates containing single mutant alleles. Likewise, heterozygous double mutant mice exhibited severe circling behavior, which was not observed in mice heterozygous for TRPML3(A419P) or PMCA2(G283S) alone. Our results provide a molecular rationale for the delayed hair cell loss in varitint-waddler mice. They also show that hair cells are able to survive for weeks with sustained Ca^{2+} loading, which implies that Ca^{2+} loading is an unlikely primary cause of hair cell death in ototoxic stress situations.

Varitint-waddler (*Va*) mice express a mutant isoform (A419P) of the transient receptor potential channel TRPML3 (murine gene symbol, *Mcoln3*) that results in profound hearing loss, vestibular defects (circling behavior, imbalance, head bobbing, waddling), pigmentation deficiencies, sterility, and perinatal lethality in homozygous animals (1). A second *Mcoln3* variant (Va^J) that arose in the *Va* background carries two mutations (I362T and A419P) and shows a phenotype with reduced severity, particularly in heterozygous animals (1). The A419P mutation in *Va* and Va^J mice is located in transmembrane-spanning domain 5(TM5)[3] of TRPML3, where it leads to a constitutively open channel, resulting in highly elevated $[Ca^{2+}]_i$ (2–5). In contrast to the effect of the A419P mutation on TRPML3 channel activity, the single I362T mutation does not appear to affect $[Ca^{2+}]_i$ (3, 5). When combined with the A419P mutation, as found in Va^J mice, the constitutive activity of this mutant TRPML3 isoform is comparable with that of A419P alone (2–5).

Here, we show that HEK293 cells expressing TRPML3-(A419P) or TRPML3(I362T/A419P) undergo rapid apoptosis. This apoptosis is suppressed by coexpression of plasma membrane calcium ATPase type 2 (PMCA2). In varitint-waddler mice, sensory hair cells survive for weeks after birth (6), which raised the question of whether this survival could be the result of the hair cells' ability to deal with normally transient and localized Ca^{2+} influx, a feature that is centered around the high levels of mobile Ca^{2+} buffers and PMCA isoforms found in sensory hair cells (7–10). We decided to test this hypothesis *in vivo* by utilizing deaf-waddler mice that carry a mutation (G283S) in the *Atp2b2* gene encoding mutant PMCA2. Mice homozygous for PMCA2(G283S) ($Atp2b2^{dfw/dfw}$) are deaf and have poor balance (11). Compared with *Atp2b2* knock-out mice, deaf-waddler mice display a milder phenotype because PMCA2(G283S) retains 30% of its biological activity compared with the wild-type isoform (12). We found that sensory hair cell loss, hearing loss, and vestibular dysfunction were aggravated in mice carrying varitint-waddler and deaf-waddler alleles compared with animals carrying the single mutant alleles. Our results reveal that the Ca^{2+}-buffering and Ca^{2+} extrusion abilities of hair cells are powerful enough to prevent cell death for weeks, even in the presence of constitutively active TRPML3(A419P), which is able to induce rapid apoptosis in other cells.

EXPERIMENTAL PROCEDURES

Plasmid Constructs—The cDNAs encoding wild-type and mutant TRPML3 channel isoforms (3) were subcloned into pcDNA3.1 (Invitrogen). Rat PMCA2z/a cDNA plasmid (13) was provided by Dr. Peter G. Gillespie (Oregon Hearing Research Center, Portland, OR). The deaf-waddler mutant

* This work was supported, in whole or in part, by National Institutes of Health Grant DC04563.

[S] The on-line version of this article (available at http://www.jbc.org) contains supplemental Movies S1 and S2.

[1] Both authors contributed equally to this work.

[2] To whom correspondence should be addressed: Depts. of Otolaryngology and Molecular and Cellular Physiology, Stanford University School of Medicine, 801 Welch Rd., Stanford, CA 94305-5739. Tel.: 650-725-6500; Fax: 650-725-8502; E-mail: hellers@stanford.edu.

[3] The abbreviations used are: TM, transmembrane-spanning domain; PMCA, plasma membrane calcium ATPase; BAPTA, 1,2-bis(*o*-aminophenoxy)-ethane-*N*,*N*,*N*′,*N*′-tetraacetic acid; P, postnatal day; ABR, auditory brainstem response; TRITC, tetramethylrhodamine isothiocyanate; IHC, inner hair cell; OHC, outer hair cell; rpm, rounds/min.

PMCA2 isoform was generated from rat PMCA2z/a cDNA plasmid using the QuikChange site-directed mutagenesis kit (Stratagene, La Jolla, CA). All plasmid cDNAs were verified by sequencing both strands entirely. GeneJammer transfection reagent (Stratagene) was used to introduce plasmid DNA for transient expression into HEK293, HeLa, and NIH3T3 cells (American Type Culture Collection, Manassas, VA).

Calcium Imaging and Electrophysiology—HEK293 cells were maintained in Eagle's minimal essential medium (Invitrogen) supplemented with 10% fetal bovine serum (Invitrogen), 100 μg/ml penicillin, and 100 μg/ml streptomycin in a humidified 5% CO_2 and 95% air atmosphere at 37 °C. Measurements of $[Ca^{2+}]_i$ with the fluorescent indicator fura-2/AM (Invitrogen) were performed using a monochromator-based imaging system (iMic platform and Polychrome V monochromator, TILL Photonics, Munich, Germany). HEK293 cells were loaded with 4 μM fura-2/AM in imaging solution containing 138 mM NaCl, 6 mM KCl, 2 mM $MgCl_2$, 2 mM $CaCl_2$, 10 mM HEPES, and 5.5 mM D-glucose (adjusted to pH 7.4 with NaOH). A 100 mM stock solution of sodium orthovanadate (Sigma) was made in sterile water. For fluorescence measurements, the cells were plated onto glass coverslips. Whole-cell currents were recorded 12–15 h after transfection with an Axopatch 200B amplifier (Axon Instruments, Sunnyvale, CA) and acquired with jClamp software (SciSoft Co., New Haven, CT). The standard bath solution contained 138 mM NaCl, 5.4 mM KCl, 2 mM $MgCl_2$, 2 mM $CaCl_2$, 10 mM HEPES, and 10 mM D-glucose (pH 7.4). The pipette solution contained 140 mM CsCl, 10 mM HEPES, 3 mM NaATP, 1 mM BAPTA, and 2 mM $MgCl_2$ (pH 7.2). 100 μM 2-aminoethyldiphenyl borate was included in the bath solution to block gap junctions. 2-Aminoethyldiphenyl borate had no effect on the expressed channels.

Mice and Genotyping—Homozygous deaf-waddler mice (C3H/HeJ-Atp2b2^{dfw}/J, stock number 001276), CH3/HeJ wild-type mice (stock number 000659), and heterozygous varitint-waddler (*Va*) mice (RSV/LeJ, stock number 000268) were obtained from The Jackson Laboratory (Bar Harbor, ME). Genomic DNA was isolated from P3–P5 mouse tails using a DNeasy blood and tissue kit (Qiagen, Valencia, CA). For PCR amplification of *Mcoln3* and *Atp2b2* genomic DNA fragments, the following primer pairs were used: 5′-TCTCACAAGCTATGATGTCTGCAG-3′ (sense) and 5′-CTGAAACTGTGAGCCAGCCCCAGT-3′ (antisense) for *Mcoln3* (400-bp fragment) and 5′-GTAACCGGGTTATACCTTCCTCAG-3′ (sense) and 5′-AAATGTGTGTGTGTAGGAGGCTTA-3′ (antisense) for *Atp2b2* (180-bp fragment). The respective PCR fragments were gel-purified (Qiagen gel extraction kit) and sequenced using the following primers: 5′-GATACCTGGGTTTCTTTGCGAAGT-3′ (*Mcoln3*) and 5′-ACCCATGTGATGGAGGGCTCAGGA-3′ (*Atp2b2*).

Auditory Brainstem Response (ABR) Measurements—For stimulus generation, presentation, and ABR acquisition, the Intelligent Hearing System and Smart-EP software (Intelligent Hearing System, Miami, FL) were used. Mice were anesthetized intraperitoneally with 100 mg/kg ketamine and 20 mg/kg xylazine. Body temperature was maintained at 37 °C by placing the mice on an isothermal pad during testing and recovery from anesthesia. Positive, negative, and ground electrodes (Model F-E2, Astro-Med, West Warwick, RI) were inserted subcutaneously at the vertex, mastoid, and back, respectively. High frequency transducers were used to generate specific acoustic stimuli (clicks or tone bursts of different frequencies). Alternating click stimuli of 0.1-ms duration and tone bursts at 3 ms were presented to both ears of the animals. All measurements were conducted at a presentation rate of 19.3/s with 1024 sweeps. ABRs were band pass-filtered below 100 Hz and above 3000 Hz, amplified, and averaged. ABR thresholds were obtained for each animal by reducing the stimulus intensity in 5-db steps to identify the lowest intensity at which all ABR waves were detectable.

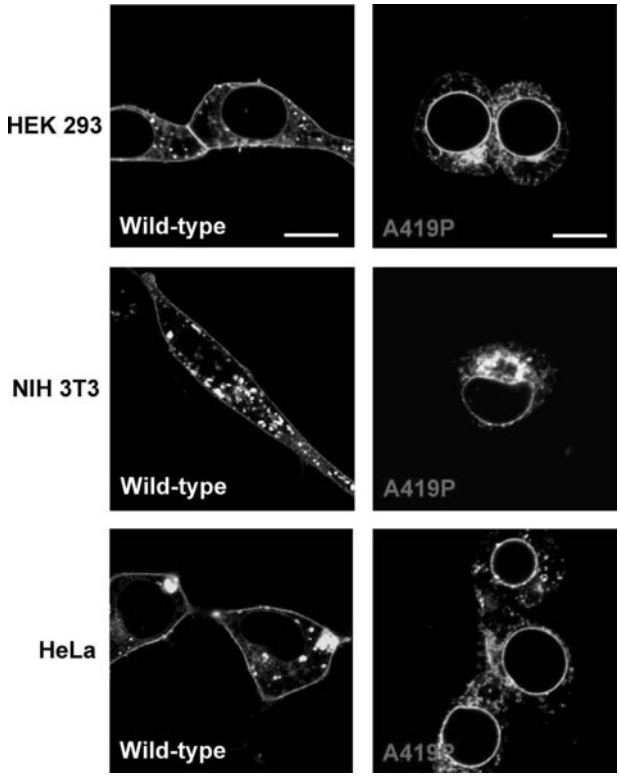

FIGURE 1. **HEK293, NIH3T3, and HeLa cells expressing either wild-type TRPML3 or the TRPML3(A419P) varitint-waddler mutant isoform.** Shown are representative cells expressing the respective C-terminal yellow fluorescent protein fusion constructs of wild-type TRPML3 and mutant TRPML3 15 h after transfection. *Scale bars* = 20 μm.

Whole-mount Immunohistochemistry—Organs of Corti and utricles were fixed with fresh 4% paraformaldehyde in phosphate-buffered saline for 1 h, permeabilized, and blocked for 1 h in buffer A (0.1% Triton X-100, 1% bovine serum albumin, and 5% heat-inactivated goat serum in phosphate-buffered saline (pH 7.3)). All steps were performed at room temperature unless indicated otherwise. After incubation overnight at 4 °C with diluted antibodies (1:1000 for rabbit anti-parvalbumin 3 polyclonal antibody (7) and 1:1000 for rabbit anti-calretinin polyclonal antibody (Chemicon, Temecula, CA)), samples were washed three times with buffer A and once with buffer B (0.1% Triton X-100 and 0.01% bovine serum albumin (w/v)). TRITC-conjugated goat anti-rabbit antibody (Jackson ImmunoResearch Laboratories, West Grove, PA) and fluorescein isothiocyanate-conjugated phalloidin (Sigma) were diluted in buffer B and incubated for 1 h. After washing once with buffer B and three

times with phosphate-buffered saline, the samples were mounted in DakoCytomation fluorescent mounting medium (Dako, Carpinteria, CA) and imaged with a confocal microscope (LSM Pascal, Zeiss, Jena, Germany).

RESULTS

TRPML3(A419P)-mediated Cell Death Is Reduced by Coexpression of PMCA2—Constitutively active TRPML3(A419P) severely affects cell morphology and survival of LLC-PK1-CL4 cells (2). We confirmed this observation by expressing TRPML3(A419P) in HEK293, NIH3T3, and HeLa cells, which rapidly acquired a rounded morphology and displayed a tendency to detach from the substrate (Fig. 1). 10 h after transfection, 25–35% of TRPML3(A419P)- and TRPML3(I362T/A419P)-expressing HEK293 cells translocated phosphatidylserine from the cytoplasmic leaflet of the plasma membrane to the cell surface (Fig. 2, *A* and *B*), which is an early diagnostic sign of apoptotic cell death that can be revealed with annexin V staining. Within the next 15 h, the number of annexin V-positive cells increased to 70%. Assuming that Ca^{2+} influx via TRPML3(A419P) and TRPML3(I362T/A419P) was the principal cause of apoptosis, we expected that coexpression of the plasma membrane calcium pump PMCA2 would lead to a reduction of annexin V-positive cells by directly counteracting the increase in $[Ca^{2+}]_i$. Indeed, the increase in annexin V-positive mutant-transfected cells was significantly reduced in the presence of PMCA2 over the examined time range of 10–25 h (Fig. 2, *A* and *B*). Wild-type TRPML3-expressing control cells were not positive for annexin V staining over the examined time period in the absence or presence of PMCA2 (Fig. 2, *A* and *B*).

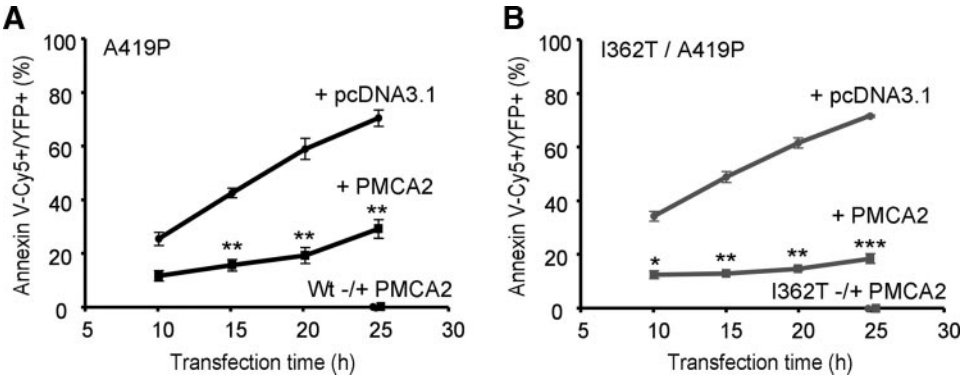

FIGURE 2. **Survival of HEK293 cells expressing varitint-waddler mutant isoforms of TRPML3 with or without PMCA2.** *A* and *B*, percentage of annexin V-positive cells at various time points (10, 15, 20, and 25 h) after cotransfection of varitint-waddler mutant isoforms of TRPML3 (C-terminally fused to yellow fluorescent protein (*YFP*)) with rat PMCA2 or empty vector (pcDNA3.1). Coexpression of wild-type (*Wt*) TRPML3 with PMCA2 or the I362T mutant isoform of TRPML3 with PMCA2 did not show any annexin V-positive staining after 25 h. These experiments were conducted in the context of a previous publication; hence, the control data shown here (*+ pcDNA3.1*) have been published previously (3). ***, $p < 0.0001$; **, $p < 0.001$; *, $p < 0.01$ (Student's *t* test, unpaired).

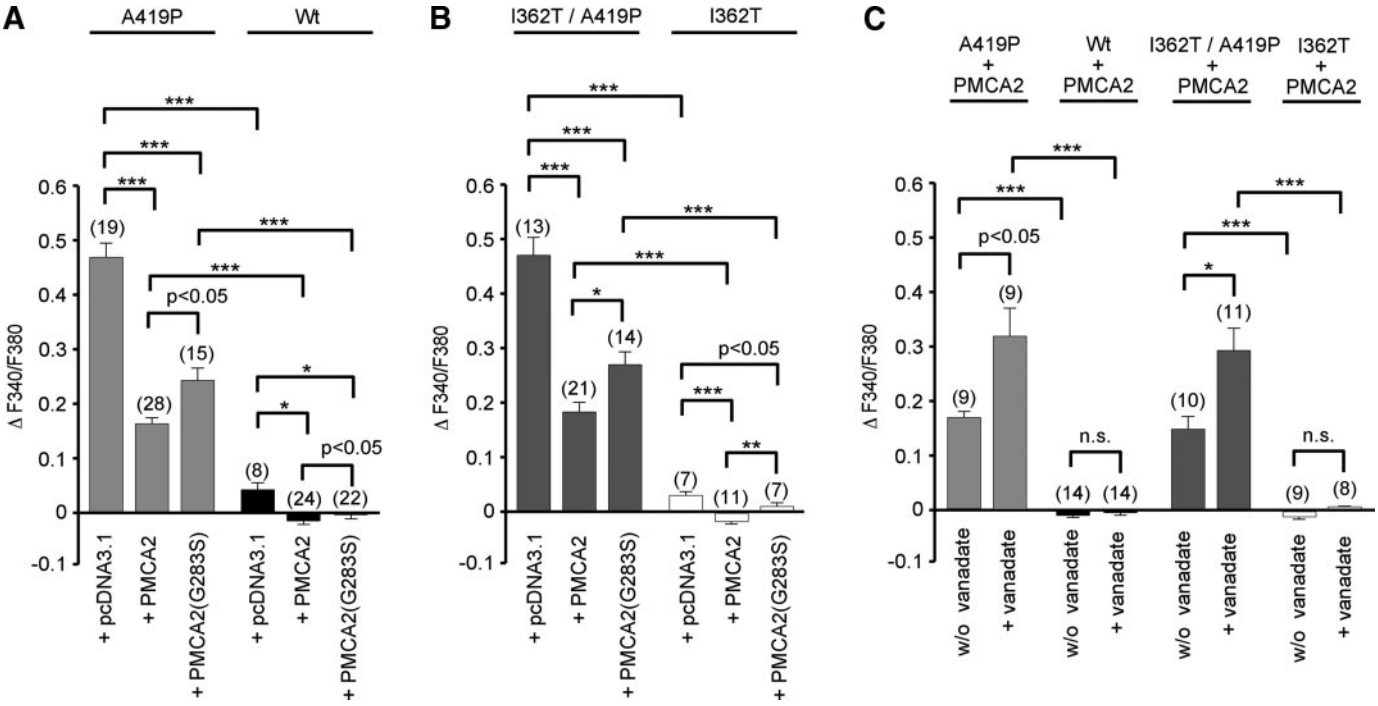

FIGURE 3. **Calcium imaging of HEK293 cells expressing varitint-waddler mutant isoforms of TRPML3 with or without PMCA2.** *A* and *B*, Ca^{2+} imaging results showing relative $[Ca^{2+}]_i$ of HEK293 cells coexpressing wild-type (*Wt*) TRPML3, the I362T mutant isoform, or varitint-waddler isoforms in combination with PMCA2, the PMCA2 deaf-waddler mutant isoform (G283S), or empty vector (pcDNA3.1). All expression vectors were cotransfected at molar ratios of 1:1. Values are the means ± S.E. (*n* shown in *parentheses*). All measurements were performed 15 h after transfection. *C*, Ca^{2+} imaging experiments as described for *A* and *B* using 1 mM sodium vanadate to block the PMCA2 effect. Cultured cells were preincubated with 1 mM sodium vanadate for 4 h before measuring. ***, $p < 0.0001$; **, $p < 0.001$; *, $p < 0.01$ (Student's *t* test, unpaired); *n.s.*, not significant. Mean values are the result of *n* independent measurements with 10–20 cells each. All mean values were corrected for the values of non-transfected control cells in each measurement.

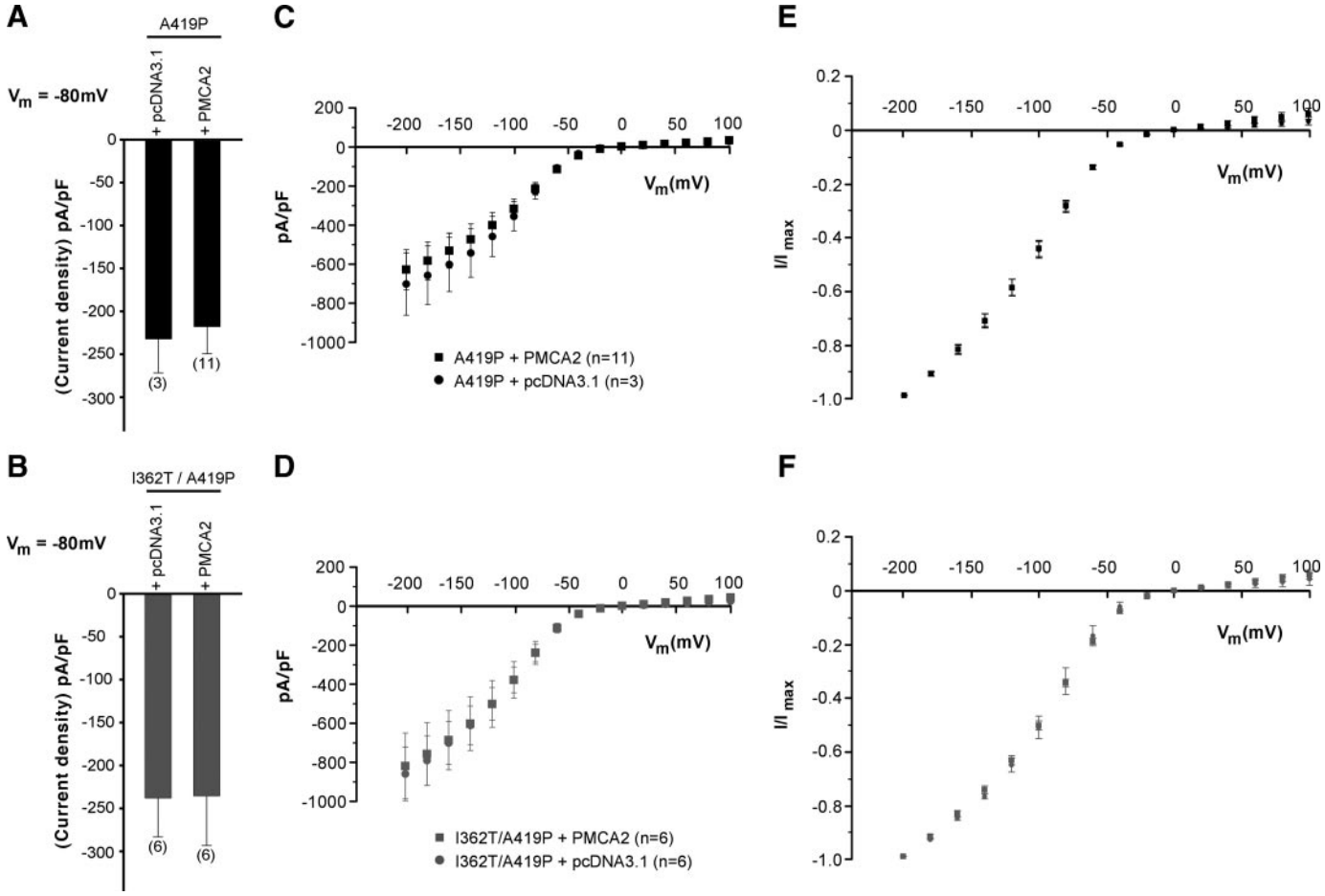

FIGURE 4. **Constitutively active conductance elicited by varitint-waddler TRPML3 mutants in HEK293 cells in the presence and absence of PMCA2.** *A* and *B*, average inward current densities at −80 mV of the murine A419P and I362T/A419P mutants, respectively, in the presence of rat PMCA2 compared with cotransfections with empty vector cDNA (pcDNA3.1), normalized by cell capacitance (picofarads (*pF*)). All expression vectors were cotransfected at molar ratios of 1:1. *n* is the number of cells analyzed. *C* and *D*, steady-state current-voltage plots of whole-cell currents elicited in cells cotransfected with the murine A419P and I362T/A419P mutants, respectively, and rat PMCA2 or empty vector cDNA in response to 10-ms voltage steps from a holding potential of +10 mV between −200 and +100 mV in 20-mV incremental steps, normalized by cell capacitance. *E* and *F*, same plot but normalized to maximal current elicited at −200 mV to demonstrate similarity in responses.

Coexpression of PMCA2 Reduces Steady-state $[Ca^{2+}]_i$ in TRPML3(A419P)-expressing Cells—Coexpression of PMCA2 with the varitint-waddler mutant isoforms of TRPML3 significantly decreased $[Ca^{2+}]_i$ in HEK293 cells compared with cells that coexpressed TRPML3 mutants with control plasmid (Fig. 3, *A* and *B*). The ameliorating effect of PMCA2 on cell death is therefore likely due to the decrease in $[Ca^{2+}]_i$ in cells coexpressing both PMCA2 and TRPML3(A419P) or PMCA2 and TRPML3(I362T/A419P) compared with controls. In agreement with a highly efficient Ca^{2+} extrusion mediated by PMCA2, we observed that cells expressing wild-type TRPML3 or the control mutant isoform TRPML3(I362T) showed a significant decrease in base-line $[Ca^{2+}]_i$ in the presence of PMCA2 compared with cells cotransfected with wild-type TRPML3 or TRPML3(I362T) and empty vector pcDNA3.1 (Fig. 3, *A* and *B*). Coexpression of either TRPML3(A419P) or TRPML3-(I362T/A419P) with the less active deaf-waddler isoform PMCA2(G283S) resulted in significantly diminished effects on $[Ca^{2+}]_i$ compared with coexpression of wild-type PMCA2 (Fig. 3, *A* and *B*). Blocking wild-type PMCA2 with 1 mM sodium vanadate (14) 4 h prior to calcium imaging measurements caused a significant increase in $[Ca^{2+}]_i$ in cells coexpressing either TRPML3(A419P) or TRPML3(I362T/A419P) with PMCA2 compared with non-treated controls (Fig. 3*C*). To exclude a direct effect of PMCA2 on the subcellular localization of TRPML3, we performed surface biotinylation experiments to detect potential changes in the plasma membrane localization of TRPML3. We found that PMCA2 did not alter the respective amounts and ratios of wild-type or mutant TRPML3 isoforms in the plasma membrane (data not shown). In addition, confocal microscopy revealed no apparent differences in the subcellular localization of wild-type or mutant TRPML3 isoforms in the presence or absence of PMCA2 (data not shown). Whole-cell currents elicited in cells coexpressing varitint-waddler mutant TRPML3 channels and PMCA2 were not significantly different from currents elicited in cells cotransfected with mutant channel isoforms and empty pcDNA3.1 vector (Fig. 4, *A–F*). These results and control experiments show that PMCA2 does not directly alter TRPML3(A419P), thereby supporting the hypothesis that the rescue effect of PMCA2 is caused by counteracting the Ca^{2+} influx from mutant TRPML3 isoforms through enhanced Ca^{2+} extrusion. Increased $[Ca^{2+}]_i$ is consequently the underlying basis for rapid apoptosis of HEK293 and other cells expressing TRPML3(A419P).

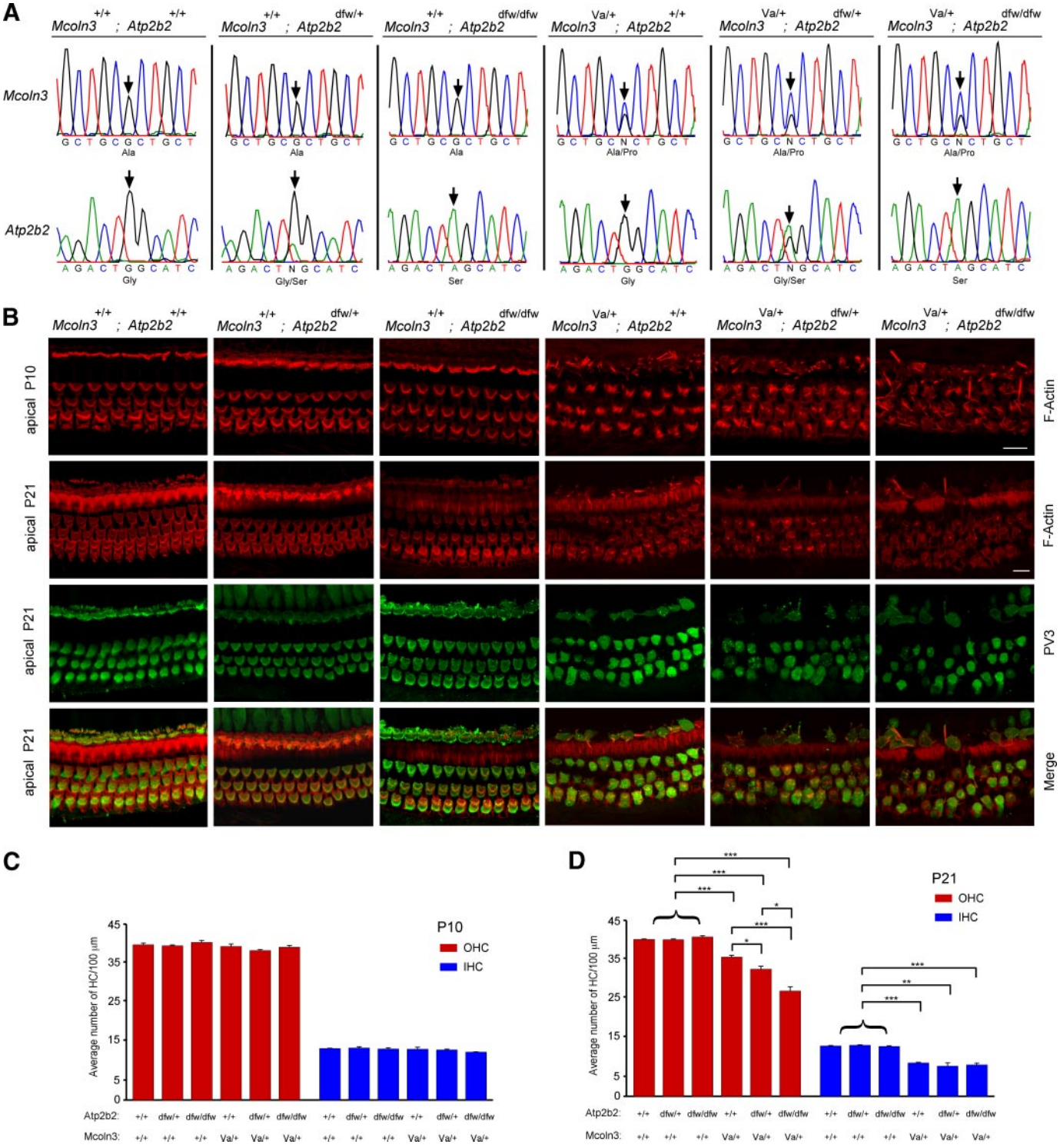

FIGURE 5. **Genotyping and analysis of cochlear hair cell degeneration in P10 and P21 varitint-waddler, deaf-waddler, and varitint-waddler/deaf-waddler double mutant mice.** *A*, genotyping results showing genomic DNA sequence traces of wild-type mice, mice heterozygous for *Va* (*Mcoln3*$^{Va/+}$), and mice hetero- and homozygous for deaf-waddler (*Atp2b2*$^{dfw/+}$ and *Atp2b2*$^{dfw/dfw}$), as well as DNA sequences of double mutant animals (*Mcoln3*$^{Va/+}$;*Atp2b2*$^{dfw/+}$ and *Mcoln3*$^{Va/+}$;*Atp2b2*$^{dfw/dfw}$). Respective DNA sequence changes take place at position 1255 (G → C) of *Mcoln3* (varitint-waddler) and at position 847 (G → A) of *Atp2b2* (deaf-waddler). *B*, hair cell bundle degeneration in P10 and P21 mice as genotyped in *A*. Shown are IHCs and OHCs from apical whole-mount preparations labeled with phalloidin (F-actin) and anti-parvalbumin 3 antibody (*PV3*). *Scale bars* = 10 µm. *C*, quantification of hair cell (*HC*) numbers at P10. *D*, quantification of hair cell numbers at P21. Shown are the average numbers of IHCs and OHCs in the apical part of the cochlea (hair cells/100 µm, means ± S.E. of at least three independent samples each). ***, $p < 0.0001$; **, $p < 0.001$; *, $p < 0.01$ (Student's *t* test, unpaired).

Deaf-waddler PMCA2 Aggravates Degeneration of Varitint-waddler Cochlear Hair Cells—To investigate the deaf-waddler mutant PMCA2 effect on varitint-waddler inner ear hair cell morphology and survival *in vivo*, we investigated cochlear whole-mount preparations of P10 and P21 mice carrying single varitint-waddler and deaf-waddler alleles as well as double

mutants. Deaf-waddler mice carrying the G283S mutation for PMCA2 were crossed with heterozygous varitint-waddler mice (*Mcoln3*$^{Va/+}$). The resulting offspring were genotyped by sequence analysis (Fig. 5*A*). We analyzed whole-mount preparations of the organs of Corti of all viable allelic combinations for overall hair cell morphology and hair cell numbers at P10 and at P21 (Fig. 5, *B* and *C*). Inner and outer hair cells of the apical, medial, and basal parts of the cochlea were examined. At P10, no significant hair cell loss was observed in any of the preparations. However, air bundles appeared to be more severely affected in *Mcoln3*$^{Va/+}$;*Atp2b2*$^{dfw/+}$ and *Mcoln3*$^{Va/+}$;*Atp2b2*$^{dfw/dfw}$ mice than in control mice carrying solely the varitint-waddler mutant allele (*Mcoln3*$^{Va/+}$;*Atp2b2*$^{+/+}$), which showed a mild hair bundle phenotype. Hair bundle morphology, as well as the number of hair cells/100-μm organ of Corti segment, in *Mcoln3*$^{+/+}$;*Atp2b2*$^{dfw/+}$ and *Mcoln3*$^{+/+}$;*Atp2b2*$^{dfw/dfw}$ mice was not different from that in wild-type mice at P10 and at P21 (Fig. 5, *B–D*). At P21, the number of inner (IHCs) and outer (OHCs) hair cells was significantly reduced in all mice carrying the varitint-waddler mutation (*Mcoln3*$^{Va/+}$;*Atp2b2*$^{+/+}$, *Mcoln3*$^{Va/+}$;*Atp2b2*$^{dfw/+}$, and *Mcoln3*$^{Va/+}$;*Atp2b2*$^{dfw/dfw}$) compared with *Mcoln3*$^{+/+}$;*Atp2b2*$^{dfw/dfw}$ mice (Fig. 5, *B* and *D*). Overall, hair bundle and OHC numbers were increasingly more affected starting with the mildest phenotype in *Mcoln3*$^{Va/+}$;*Atp2b2*$^{+/+}$ mice, followed by *Mcoln3*$^{Va/+}$;*Atp2b2*$^{dfw/+}$, and finally *Mcoln3*$^{Va/+}$;*Atp2b2*$^{dfw/dfw}$ mice, which displayed the most severe phenotype. The number of IHCs was significantly reduced in all preparations containing the *Mcoln3*$^{Va/+}$ allele, but in contrast to the OHCs, the IHCs did not appear to be significantly affected by the presence of the deaf-waddler allele. This IHC result might be explained by the lower expression of PMCA2 in IHCs compared with OHCs (8). In general, our results demonstrate that the addi-

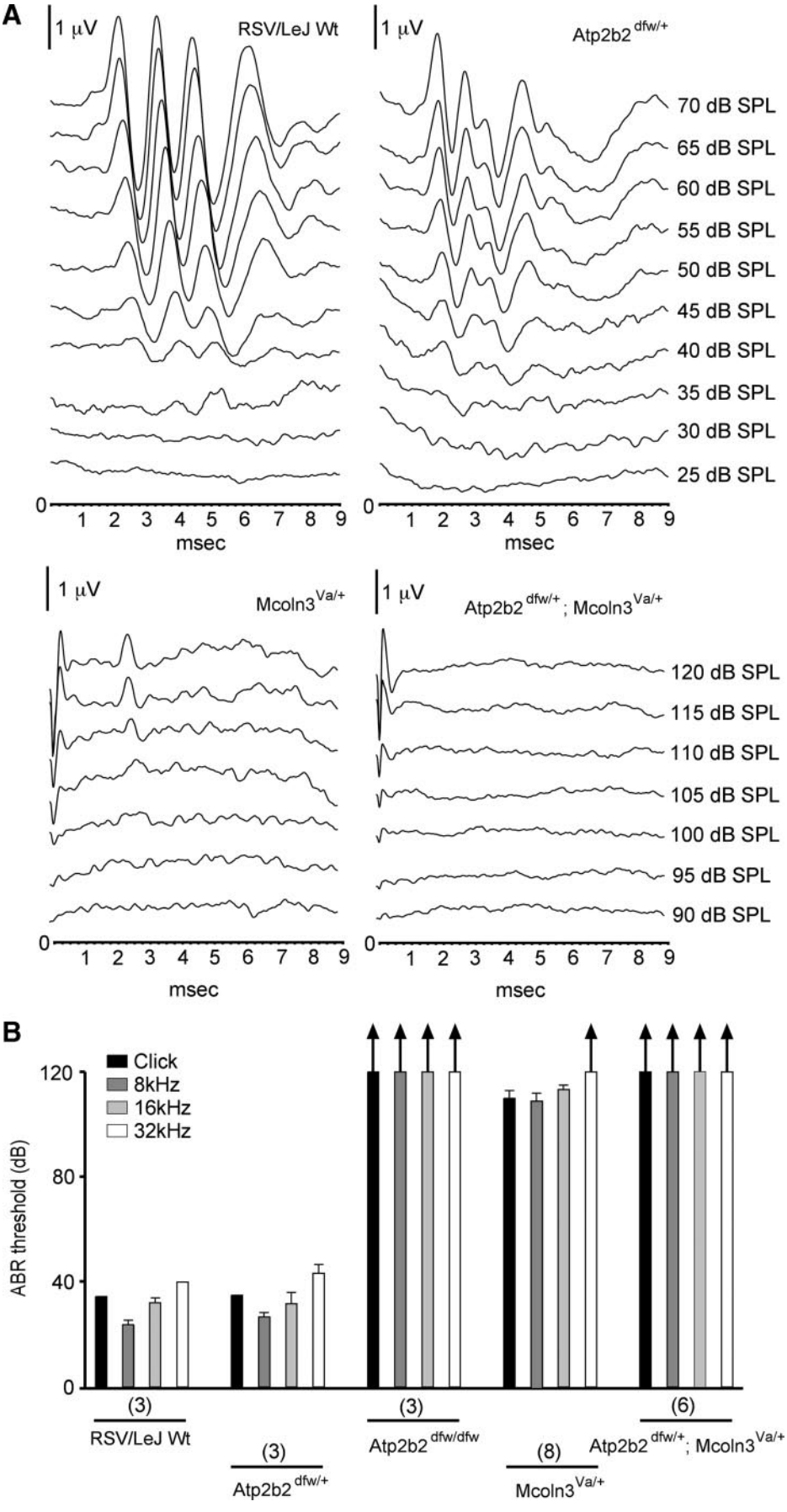

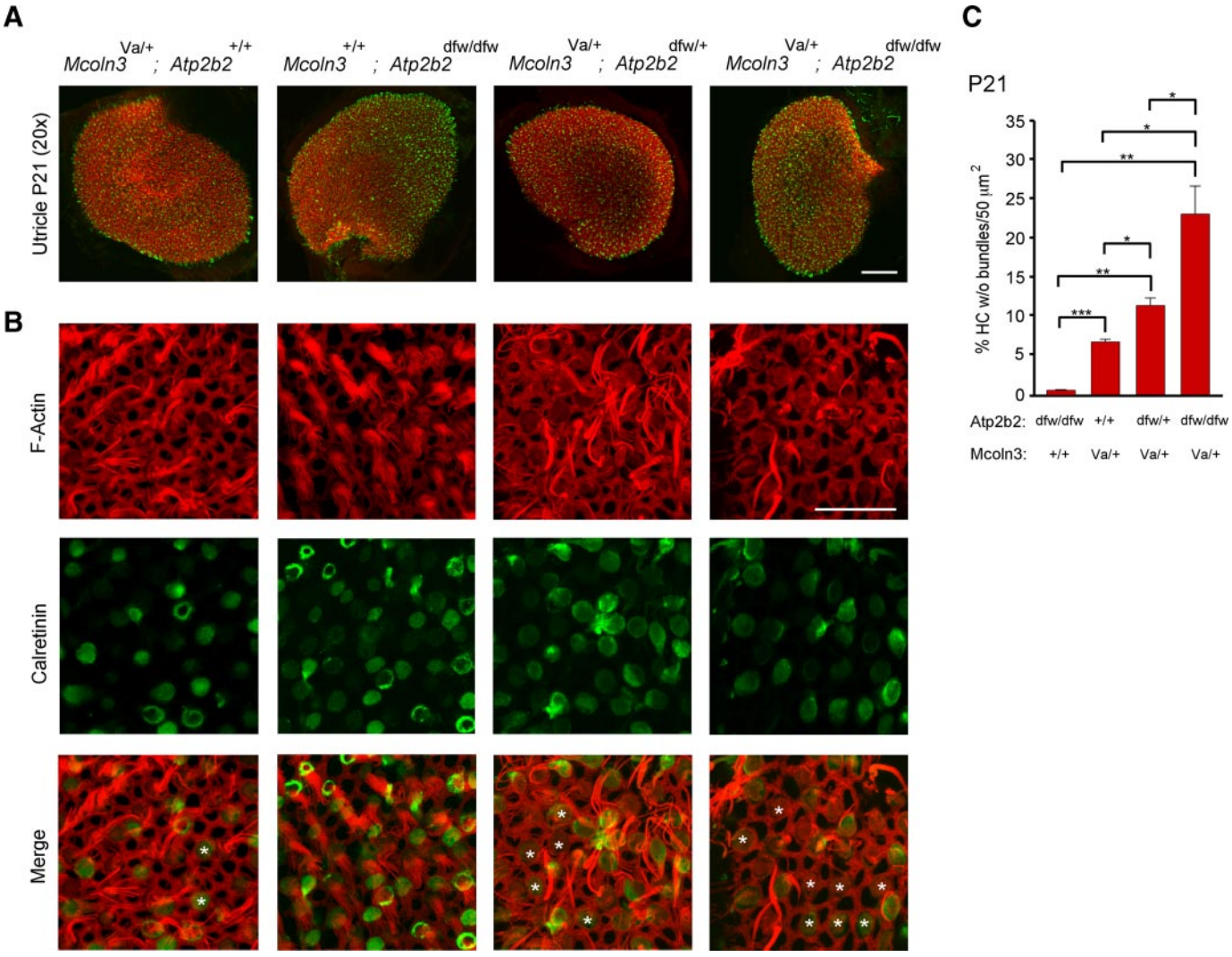

FIGURE 7. **Analysis of vestibular hair cell degeneration in varitint-waddler, deaf-waddler, and varitint-waddler/deaf-waddler double mutant mice.** *A* and *B*, representative immunofluorescence stainings of P21 murine utricle preparations. The higher magnification examples (*B*) are from comparable areas in the striola region, where the phenotype was most noticeable. Preparations were stained with phalloidin (F-actin) and anti-calretinin antibody. *Asterisks* indicate hair cells without bundles. *Scale bars* = 100 μm (*A*) and 20 μm (*B*). *C*, percentage of hair cells (*HC*) without bundles at P21 in the striola region of the utricle (hair cells/50 μm^2, means ± S.E. of at least three independent samples each). ***, $p < 0.001$; **, $p < 0.01$; *, $p < 0.05$ (Student's *t* test, unpaired).

tion of deaf-waddler mutant alleles successively enhances the varitint-waddler phenotype in OHCs of the organ of Corti.

Auditory-evoked Brainstem Response Measurements of Varitint-waddler/Deaf-waddler Double Mutants—Auditory-evoked brainstem response measurements were used to evaluate hearing thresholds of P21 mice. Mice homozygous for PMCA2(G283S) ($Mcoln3^{+/+}$;$Atp2b2^{dfw/dfw}$) were all profoundly deaf; no waveform was observed, even to sound stimuli of 120 db of sound pressure (Fig. 6*B*). Similarly, the double mutants $Mcoln3^{Va/+}$;$Atp2b2^{dfw/+}$ and $Mcoln3^{Va/+}$;$Atp2b2^{dfw/dfw}$ were also profoundly deaf (Fig. 6, *A* and *B*) (data not shown). On the other hand, ABRs were measurable in $Mcoln3^{Va/+}$;$Atp2b2^{+/+}$ and $Mcoln3^{+/+}$;$Atp2b2^{dfw/+}$ mice (Fig. 6, *A* and *B*). ABR thresholds for $Mcoln3^{Va/+}$;$Atp2b2^{+/+}$ mice were 109 ± 3 and 113 ± 1 db of sound pressure for 8- and 16-kHz tone bursts, respectively, and 111 ± 1 db of sound pressure for click stimuli ($n = 8$) (Fig. 6*B*), measurements that are in agreement with those in a previous report (15). The results for $Mcoln3^{+/+}$;$Atp2b2^{dfw/+}$ mice are in accordance with previous findings of no significant differences in comparison with wild-type controls (16). However, the addition of a single deaf-waddler allele to the varitint-waddler allele exaggerated the phenotype, which resulted in complete deafness of $Mcoln3^{Va/+}$;$Atp2b2^{dfw/+}$ mice at P21 (Fig. 6, *A* and *B*).

Deaf-waddler PMCA2 Aggravates Degeneration of Varitint-waddler Utricle Hair Cells—The clear effects on cochlear hair bundle morphology and OHC numbers elicited by combining one or both deaf-waddler alleles with the heterozygous varitint-waddler mutation raised the question of whether reducing PMCA2 activity would also affect the vestibular system. We

FIGURE 6. **ABR measurements.** *A*, shown are representative ABRs of 3-week-old wild-type (*Wt*; RSV/LeJ), heterozygous varitint-waddler ($TRPML3^{Va/+}$), heterozygous deaf-waddler ($PMCA2^{dfw/+}$), and varitint-waddler/deaf-waddler double mutant ($TRPML3^{Va/+}$;$PMCA2^{dfw/+}$) mice to a click stimulus. *SPL*, sound pressure level. *B*, shown are ABR thresholds (means ± S.E.) to click and 8-, 16-, and 32-kHz stimuli (n = number of animals).

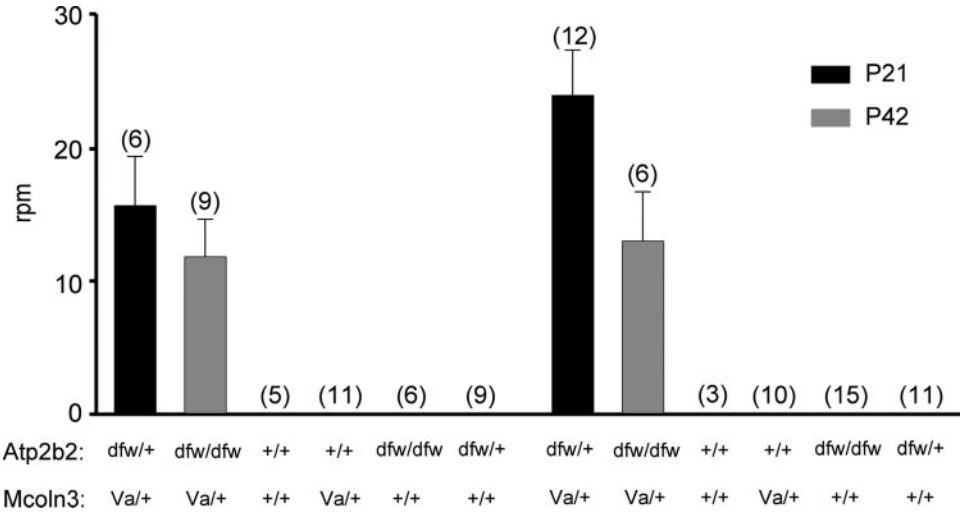

FIGURE 8. **Circling behavior of varitint-waddler/deaf-waddler double mutant mice.** The quantification was conducted at 3 and 6 weeks postnatal (P21 and P42, respectively). Wild-type littermates (RSV/LeJ), heterozygous varitint-waddler mice (*Mcoln3*$^{Va/+}$;*Atp2b2*$^{+/+}$), and PMCA2(G283S) mutant mice (*Mcoln3*$^{+/+}$;*Atp2b2*$^{dfw/+}$ and *Mcoln3*$^{+/+}$;*Atp2b2*$^{dfw/dfw}$) did not display circling behavior at P21 and P42 (n = number of mice tested). 67% (n = 6/9, P21) and 71% (n = 12/17, P42) of the heterozygous double mutants (*Mcoln3*$^{Va/+}$;*Atp2b2*$^{dfw/+}$) and 100% (n = 9/9, P21; n = 6/6, P42) of the *Mcoln3*$^{Va/+}$;*Atp2b2*$^{dfw/dfw}$ double mutants showed severe circling behavior. Non-circling mice were excluded from rpm calculations. For each mouse, we quantified circling of three tests that were performed at consistent time points on different days.

consequently analyzed P21 mouse utricle sensory epithelia, and although we did not find a striking effect on hair cell numbers at this age, we noticed effects on hair bundle morphology. At P21, *Mcoln3*$^{+/+}$;*Atp2b2*$^{dfw/+}$ and *Mcoln3*$^{+/+}$;*Atp2b2*$^{dfw/dfw}$ utricles were not different from the respective wild-type organs (RSV/LeJ and CH3/HeJ) (Fig. 7) (data not shown). Hair bundles of *Mcoln3*$^{Va/+}$;*Atp2b2*$^{+/+}$ utricles were disorganized and splayed, and some hair cells appeared to lack a hair bundle. Hair bundles of *Mcoln3*$^{Va/+}$;*Atp2b2*$^{dfw/+}$ utricles were more disorganized and degenerated, and more hair cells showed a complete lack of bundles (Fig. 7). The most severe hair bundle phenotype was detectable in *Mcoln3*$^{Va/+}$;*Atp2b2*$^{dfw/dfw}$ utricles, where hair bundles generally appeared to be thinner or were completely absent, particularly in the striola region (Fig. 7).

Lowering of PMCA2 Efficacy Causes Circling and Coordination Problems in Varitint-waddler Mutants—An obvious change that we observed when combining varitint-waddler and deaf-waddler alleles was the occurrence of circling behavior in double mutants (Fig. 8). Wild-type mice, heterozygous varitint-waddler mice (*Mcoln3*$^{Va/+}$;*Atp2b2*$^{+/+}$) or mice carrying one or both alleles of the deaf-waddler mutation (*Mcoln3*$^{+/+}$; *Atp2b2*$^{dfw/+}$ and *Mcoln3*$^{+/+}$;*Atp2b2*$^{dfw/dfw}$) did not show circling behavior during the investigated time period (up to 6 months postnatal). In contrast, 67 and 71% of the *Mcoln3*$^{Va/+}$; *Atp2b2*$^{dfw/+}$ double mutants at 3 and 6 weeks of age, respectively, and 100% of 3- and 6-week-old *Mcoln3*$^{Va/+}$;*Atp2b2*$^{dfw/dfw}$ double mutants showed overt circling behavior. *Mcoln3*$^{Va/+}$; *Atp2b2*$^{dfw/+}$ mice circled with 15.3 ± 3.9 rounds/min (rpm; mean ± S.E.) at 3 weeks of age and with 23.9 ± 3.4 rpm at 6 weeks of age. *Mcoln3*$^{Va/+}$;*Atp2b2*$^{dfw/dfw}$ mice circled with 11.7 ± 2.7 rpm at 3 weeks of age and with 12.8 ± 3.8 rpm at 6 weeks of age. The slower circling speed of *Mcoln3*$^{Va/+}$; *Atp2b2*$^{dfw/dfw}$ animals is likely due to the increased waddling phenotype, where the mice displayed severe coordination problems in addition to circling, which affected their gait (Fig. 8; see also supplemental Movie S1 (*Mcoln3*$^{Va/+}$;*Atp2b2*$^{+/+}$, *Mcoln3*$^{+/+}$; *Atp2b2*$^{dfw/+}$, and *Mcoln3*$^{Va/+}$; *Atp2b2*$^{dfw/+}$) and supplemental Movie S2 (*Mcoln3*$^{+/+}$;*Atp2b2*$^{dfw/dfw}$ and *Mcoln3*$^{Va/+}$;*Atp2b2*$^{dfw/dfw}$)).

DISCUSSION

In this study, we investigated the mechanism by which sensory hair cells are able to deal with a severe cationic overload caused by constitutive activity of the TRPML3 channel in varitint-waddler mice. We found that HEK293 and other cells that express TRPML3(A419P) undergo rapid apoptosis. Although TRPML3(A419P) is a rather non-specific cation channel (17), we concluded that it is Ca^{2+} overload that ultimately leads to apoptosis because coexpression of PMCA2 significantly alleviated the number of apoptotic HEK293 cells expressing TRPML3(A419P). This finding sheds light on why sensory hair cells of varitint-waddler mice that express a mutant TRPML3 channel already during the first postnatal week (1, 18) are able to survive for many weeks after birth.

Hair cells are endowed with unusually concentrated mobile Ca^{2+} buffers (7, 10) and highly efficient Ca^{2+} extrusion mechanisms (8, 9) that control local Ca^{2+} homeostasis in the hair bundle and at synaptic sites. We hypothesized that this ability to deal with Ca^{2+} loads allows hair cells to adapt, at least temporarily, to the otherwise devastating A419P varitint-waddler mutation of TRPML3. Varitint-waddler hair cells are clearly affected by the TRPML3(A419P) mutation, which leads to depolarization by an inwardly rectifying leak current (3, 18). Beside Ca^{2+}-buffering and Ca^{2+} extrusion abilities, hair cells appear to down-regulate expression of the mutant TRPML3 channel (18), potentially via reduced surface expression of the mutant channel, a result we found in HEK293 cells, where we estimated a two-third reduction in surface expression of the mutant channel compared with the wild-type channel (3).

To test our hypothesis, we used the naturally occurring deaf-waddler mutation, which severely hampers the Ca^{2+}-pumping ability of PMCA2. We proposed that a slight reduction in the Ca^{2+} extrusion ability of hair cells would increase the severity of the varitint-waddler phenotype. Specifically, we expected double mutants to show more severe hair bundle defects and more extensive hair cell loss than their respective single mutants. We selected the deaf-waddler mutation because its heterozygous phenotype is relatively mild compared with the phenotype of the heterozygous varitint-waddler mutation. The observed augmentation of the cellular defects in the organs of Corti and utricles of *Mcoln3*$^{Va/+}$;*Atp2b2*$^{dfw/+}$ double mutants supported our hypothesis. These results indicated that a reduction of PMCA2 efficacy that normally does not lead to any cel-

lular or phenotypical defects in heterozygous animals has a severe augmenting effect on TRPML3(A419P)-expressing hair cells. As a result, *Mcoln3*$^{Va/+}$;*Atp2b2*$^{dfw/+}$ double mutants lack ABRs, even when stimulated with 120 db of sound pressure, which is a more severe phenotype than that detected in the corresponding single mutant littermates. Likewise, we observed a behavioral phenotype in *Mcoln3*$^{Va/+}$;*Atp2b2*$^{dfw/+}$ double mutant animals indicative of a severe vestibular dysfunction; this circling phenotype was not detectable in single mutants.

In the cochlea, the observed effect of reducing PMCA2 efficacy was significant only in OHCs, whereas IHC degeneration appeared not to be further enhanced by adding deaf-waddler alleles. A likely explanation for this is that PMCA2 is found mainly in OHCs and vestibular hair cells, but to a lesser extent in IHCs, where other PMCA isoforms are present (8).

The function of wild-type TRPML3 in hair cells is unclear. The channel protein is detectable in P2–P6 IHC and OHC stereocilia, where it localizes toward the stereociliary base (18). At P10, TRPML3 immunoreactivity appears to diminish in cochlear hair cell stereocilia (18). TRPML3 is regulated by changes in the extracellular Na^+ composition, and it is conceivable that native TRPML3 is a constitutively active channel that is blocked by Na^+ (5, 17). The composition of the endolymph, the fluid in which the hair bundles protrude, drastically changes during the first neonatal week, and the consequential decrease in [Na^+], accompanied by an increase in [K^+], could lead to activation of TRPML3 during a time that is critical for hair bundle, hair cell, and organ of Corti development.

Pathological changes in TRPML3 such as the A419P varitint-waddler mutation are useful because they potentially reveal certain aspects of hair cell pathology that could provide insight into mechanisms of hearing loss. We and others have reported that TRPML3(A419P) is constitutively active. This channel pathology was initially thought to be due to a simple change in the topology of TM5, which was proposed to affect the channel's pore (3, 5). Recently, it was suggested that, in addition to structural changes in the pore region due to the A419P mutation, structural features of the extracellular loop between TM1 and TM2 might be functionally involved in the constitutive activity of TRPML3(A419P) and that disruption of this regulation by protons could lock the mutant channel in an open state (17). In any case, the result of the A419P mutation is constitutive TRPML3 activity. Here, we have shown that sensory hair cells are able to deal with such a defective TRPML3 channel, which, when overexpressed in HEK293 and other cells, results in rapid cell death. We have demonstrated that this durability to withstand sustained Ca^{2+} loads is likely due to the inherent ability of hair cells to buffer and extrude Ca^{2+}, which normally enters hair cells via active mechanoelectrical transduction channels and synaptic Ca^{2+} channels. It is surprising that these buffering and extrusion mechanisms, which are normally used to terminate and locally confine Ca^{2+} influx, are able to delay imminent cell death for several weeks. One consequential conclusion is that Ca^{2+} influx due to sustained mechanical stimulation of wild-type hair cells is not necessarily causative for hearing loss as suggested previously (19). As an alternative to sustained Ca^{2+} influx, mechanical damage of stereocilia and their rootlets (20) could play a much more pronounced role in hair cell loss, among other factors. This conclusion reveals an interesting aspect of the potential causes of hair cell and hearing loss. Our results show that even prolonged and massive Ca^{2+} loading is not immediately toxic for hair cells, which highlights that hair cell death in response to overstimulation potentially involves other, more subtle mechanisms.

Acknowledgments—We thank Drs. Zhigang Xu and Anthony W. Peng for helpful comments on the manuscript, Dr. Gerald R. Popelka for expert advice on ABR measurements, and Dr. Peter G. Gillespie for kindly providing the rat PMCA2z/a cDNA plasmid.

REFERENCES

1. Di Palma, F., Belyantseva, I. A., Kim, H. J., Vogt, T. F., Kachar, B., and Noben-Trauth, K. (2002) *Proc. Natl. Acad. Sci. U. S. A.* **99,** 14994–14999
2. Nagata, K., Zheng, L., Madathany, T., Castiglioni, A. J., Bartles, J. R., and Garcia-Anoveros, J. (2008) *Proc. Natl. Acad. Sci. U. S. A.* **105,** 353–358
3. Grimm, C., Cuajungco, M. P., van Aken, A. F., Schnee, M., Jors, S., Kros, C. J., Ricci, A. J., and Heller, S. (2007) *Proc. Natl. Acad. Sci. U. S. A.* **104,** 19583–19588
4. Xu, H., Delling, M., Li, L., Dong, X., and Clapham, D. E. (2007) *Proc. Natl. Acad. Sci. U. S. A.* **104,** 18321–18326
5. Kim, H. J., Li, Q., Tjon-Kon-Sang, S., So, I., Kiselyov, K., and Muallem, S. (2007) *J. Biol. Chem.* **282,** 36138–36142
6. Cable, J., and Steel, K. P. (1998) *Hear. Res.* **123,** 125–136
7. Heller, S., Bell, A. M., Denis, C. S., Choe, Y., and Hudspeth, A. J. (2002) *J. Assoc. Res. Otolaryngol.* **3,** 488–498
8. Dumont, R. A., Lins, U., Filoteo, A. G., Penniston, J. T., Kachar, B., and Gillespie, P. G. (2001) *J. Neurosci.* **21,** 5066–5078
9. Yamoah, E. N., Lumpkin, E. A., Dumont, R. A., Smith, P. J., Hudspeth, A. J., and Gillespie, P. G. (1998) *J. Neurosci.* **18,** 610–624
10. Edmonds, B., Reyes, R., Schwaller, B., and Roberts, W. M. (2000) *Nat. Neurosci.* **3,** 786–790
11. Street, V. A., McKee-Johnson, J. W., Fonseca, R. C., Tempel, B. L., and Noben-Trauth, K. (1998) *Nat. Genet.* **19,** 390–394
12. Penheiter, A. R., Filoteo, A. G., Croy, C. L., and Penniston, J. T. (2001) *Hear. Res.* **162,** 19–28
13. Hill, J. K., Williams, D. E., LeMasurier, M., Dumont, R. A., Strehler, E. E., and Gillespie, P. G. (2006) *J. Neurosci.* **26,** 6172–6180
14. De Luisi, A., and Hofer, A. M. (2003) *J. Cell Sci.* **116,** 1527–1538
15. Kim, H. J., Jackson, T., and Noben-Trauth, K. (2003) *J. Assoc. Res. Otolaryngol.* **4,** 83–90
16. McCullough, B. J., and Tempel, B. L. (2004) *Hear. Res.* **195,** 90–102
17. Kim, H. J., Li, Q., Tjon-Kon-Sang, S., So, I., Kiselyov, K., Soyombo, A. A., and Muallem, S. (2008) *EMBO J.* **27,** 1197–1205
18. van Aken, A. F., Atiba-Davies, M., Marcotti, W., Goodyear, R. J., Bryant, J. E., Richardson, G. P., Noben-Trauth, K., and Kros, C. J. (2008) *J. Physiol. (Lond.)* **586,** 5403–5418
19. Fridberger, A., Flock, A., Ulfendahl, M., and Flock, B. (1998) *Proc. Natl. Acad. Sci. U. S. A.* **95,** 7127–7132
20. Duncan, R. K., and Saunders, J. C. (2000) *J. Comp. Physiol.* **186,** 1095–1106